First-principles study on electronic structures and phase stability of MnO and FeO under high pressure

Zhong Fang, Igor V. Solovyev, and Hideaki Sawada*
Joint Research Center for Atom Technology, Angstrom Technology Partnership, 1-1-4 Higashi, Tsukuba, Ibaraki 305-0046, Japan

Kiyoyuki Terakura
Joint Research Center for Atom Technology, National Institute for Advanced Interdisciplinary Research, 1-1-4 Higashi, Tsukuba, Ibaraki 305-8562, Japan
and Institute of Industrial Science, University of Tokyo, 7-22-1 Roppongi, Minato-ku, Tokyo 106-8558, Japan
(Received 21 May 1998)

The electronic structures and the phase stability of MnO and FeO under ultrahigh pressure were studied by the first-principles plane-wave basis pseudopotential calculations. Different crystal structures combined with different spin structures were studied systematically for both MnO and FeO with full structure optimization. The present calculations based on generalized gradient approximation (GGA) account well for the properties of MnO and FeO especially in the high-pressure region. For the low pressure regime, where the electron correlation is very strong, we performed the LDA+U calculations with the electron correlation and the spin-orbit coupling taken into account to supplement the GGA results. Our results predict that the high-pressure phase of MnO should take the metallic normal NiAs (nB8) structure rather than the B2 structure, and that a metastable nonmagnetic B1 structure with stretched distortion along the [111] direction can be realized for MnO in the intermediate pressure range. A unique antiferromagnetic inverse NiAs (iB8) structure as the high-pressure phase of FeO was discussed in detail, and the uniqueness was made clearer by comparing with the FeS case. The distortions and the magnetic moments for different phases were characterized. The larger c/a ratios for both nB8 MnO and iB8 FeO can be explained based on our analysis of the cation-radius/anion-radius ratio versus c/a for series of related materials. [S0163-1829(98)01246-6]

I. INTRODUCTION

The transition-metal monoxides (TMMO), with the rock salt (B1) structure at ambient condition, have occupied a special position in condensed-matter physics for decades as a prototypical example of the Mott insulators.[1] They served as standard systems for the study of the basic natures of insulating state, super-exchange and orbital magnetism. The basic properties of TMMO are specified by the electron correlation whose strength is measured by U/W with U the effective Coulomb interaction intergral between d electrons and W the d-band width. Another important quantity is Δ/W with Δ the electron excitation energy from the oxygen p-states to the transition metal d states. As the d band width is most directly controlled by pressure, the high-pressure studies of TMMO have been regarded as a useful way to understand their basic properties. Insulator-metal transition, magnetic moment collapse and so on are possible transitions which may happen under high pressure. In addition to them, structural phase transitions induced by pressure are also an attractive subject. Particularly for FeO, its stable high pressure phase may have an important implication in the earth science because FeO is one of the basic oxide components in the interior of the Earth.

For both MnO and FeO, antiferromagnetic (with type-II) rhombohedrally distorted B1 phases, called AF rB1 hereafter, are observed experimentally under ambient pressure, when temperature is decreased below the Néel temperature. However, there is a difference between MnO and FeO. The rocksalt cell is compressed along a body diagonal for MnO[2] while stretched for FeO.[3,4] The AF spin ordering is such that all transition-metal (TM^{2+}) ions in planes perpendicular to the [111] direction of the rocksalt cell have the same spin alignment, and the spins between nearest-neighboring planes are antiparallel. With increasing pressure, the rhombohedral distortion for FeO in the AF state is enhanced (more stretched).[4] However, a very recent experiment showed that the rhombohedral distortion for MnO in the AF state will be more compressed with increasing pressure.[2]

A recent shock compression experiment on MnO showed the existence of a possible high-pressure phase above 90 GPa,[5] though some earlier static high-pressure experiments on MnO indicated an absence of the high-pressure phase up to pressure of 90 GPa at room temperature.[6,7] However, the crystal structure of the high pressure phase of MnO has not been determined yet. Considering the fact that almost all of the alkaline-earth monoxides with the B1 structure at normal pressure undergo structure phase transitions from the B1 to the CsCl type (B2) structure or distorted B2 structure at high pressure[8–11] except MgO which remains in the B1 structure up to 230 GPa,[12] it was speculated that the high-pressure phase of MnO may take the B2 structure. The speculation was based on the observation that in the plane of the critical pressures versus cation ionic radius, alkaline-earth monoxides except MgO are connected by a smooth line and that MnO is located at a smoothly extrapolated part of this line (while FeO is clearly off the line).[5] More recently, a high pressure experiment with static compression at room tem-

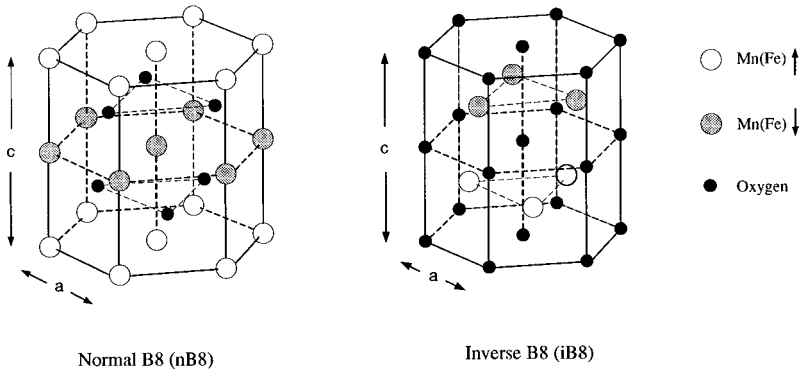

FIG. 1. Comparision of AF normal B8 (nB8) and inverse B8 (iB8) structures. Oxygen is denoted by a small black filled circle, Mn (or Fe) with up spin by a large open circle, and Mn (or Fe) with down spin by a large gray filled circle. These two structures are definitely different, and there is no inversion symmetry for the AF iB8 structure.

perature was performed for MnO up to 137 GPa and x-ray diffraction patterns were obtained for various pressures.[2] Indeed, this static compression experiment reproduced the phase transition. Moreover, the x-ray diffraction patterns obtained by this static compression experiment seem to suggest that there exist some intermediate-pressure phases within the pressure range of 90–120 GPa. However, the x-ray diffraction cannot give us an unambiguous answer about the crystal structures of the high-pressure phase and also of the intermediate-pressure phases because of the limited range of diffraction angle and moreover multiphase coexistence.

In the case of wüstite ($Fe_{1-x}O$), shock compression experiments indicated the existence of a pressure induced phase transition at about 70 GPa,[13,14] though the static compression experiment by the diamond-anvil cell at room temperature did not detect this phase transition up to 120 GPa.[4] Metallic behavior of $Fe_{1-x}O$ has been observed at static pressure and elevated temperatures[15] and also in shock resistivity measurements,[16] around the pressure range at which the phase change was observed under shock compression. This high-pressure phase of $Fe_{1-x}O$ was recently assigned to be the NiAs (B8) type structure by the analysis of x-ray diffraction peak positions.[17,18] On the analogy of most of the transition-metal compounds with the B8 structure, a natural idea for the B8 FeO may be such that Fe occupies the Ni site and O the As site. This structure is named normal B8 (nB8 for short) hereafter. However, another structure, which is named inverse B8 (iB8), is possible by exchanging the Fe and O positions. The comparison between nB8 and iB8 structures is shown in Fig. 1. The two structures are different in general and moreover have different symmetries for the AF order case. To the best of our knowledge, no transition-metal compounds have ever been known to take the iB8 structure. Actually the intensity profile of the observed x-ray diffraction pattern for $Fe_{1-x}O$ is not consistent with the nB8 structure, though both structures will give the same x-ray diffration peak positions if the lattice parameters are the same. The iB8 structure was first mentioned in the work by Cohen *et al.*[19] without any judgement on the relative stability between the nB8 and iB8 structures.

Recent progresses on the first-principles density functional theory[20] (DFT) makes it a powerful tool to predict the high-pressure behavior of many systems[21–23] and make it possible to provide us with valuable hints to the problems mentioned above. Isaak *et al.*[24] investigated the phase stability and physical properties of stoichiometric wüstite (FeO) at high-pressure based on the local-density approximation[25] (LDA). However, only B1 and B2 structures were studied, and their calculation predicted that the phase transition from AF rB1 to B2 will happen at very high pressure (around 500 GPa) for FeO. The possible collapse of magnetic moment in TMMO under high-pressure was also predicted by Cohen *et al.*[19] based on the generalized gradient approximation[26] (GGA). Recently, the possible pressure induced phase transition of FeO from B1 to nB8 structure was studied by Sherman *et al.*[27] based on the GGA. Only ferromagnetic (FM) nB8 FeO was studied in this work, and the transition from B1 to FM nB8 was estimated to happen at about 130 GPa at 0 K. Based on the assumption that the high-pressure phase of FeO has the nB8 structure, the metallic nature of the FeO (nB8 phase) was argued by Sherman *et al.*[28] as a result of breakdown of the Mott insulating condition. However, the relative stability of iB8 struture with respect to nB8 remains unsolved. Contrasting to the case of FeO, no calculations on the high-pressure behavior of MnO have been reported to our knowledge.

To extend our previous study[29] which claimed that the iB8 and nB8 should be the high-pressure phases of FeO and MnO, respectively, the detailed electronic structures and the phase stability of MnO and FeO under high-pressure, which reaches the range in the Earth's lower mantle, are studied systematically in the present work with the first-principles calculations. Different crystal structures (B1, B2, nB8, iB8) and spin structures [AF, FM, nonmagnetic (NM)] are studied for both MnO and FeO with full structure optimization, so that we can make systematic comparison. The GGA has been used for all of the calculations. However, for the low pressure regime, where the electron correlation is very strong, we performed the LDA+U calculations to supplement the GGA results. Detailed analysis of effects of the electron correlation and the spin-orbit coupling (SOC) on the ground state under normal pressure will be presented. In addition to providing some additional supports to our previous claims about the high-pressure phases of MnO and FeO, it will be shown that the almost nonmagnetic low-spin state of the rB1 structure (NM rB1 state) is one of the intermediate phases of MnO observed by the static compression experiment. In order to understand the special features of the AF iB8 phase as the high-pressure phase of FeO, the electronic structures were studied in detail. The uniqueness of this AF iB8 structure can be made clearer by comparing with the FeS case. The changes of distortions and magnetic moments of different phases with increasing pressure are also presented. The larger c/a ratios for both nB8 MnO and iB8 FeO are explained based on our analysis of the cation-radius/anion-radius ratio versus c/a for series of related materials. The

paper is organized in the following way: first a detailed description of our calculation method will be given in Sec. II, the results and discussion will be given in Sec. III, and some supplementary discussions will be presented in Sec. IV. Finally Sec. V will contribute to the summary of our results.

II. CALCULATION METHODS

In the present work, the electron-electron interaction is basically treated by GGA like in other similar calculations.[19,27] For systems where the electronic states have localized natures, the GGA gives much better results than the simpler approximation LDA. Moreover, if we concentrate on the high-pressure region, where the electron correlation is weak because of the increase of screening, a description by the GGA will be very reliable. However, the GGA is not yet powerful enough to treat the strong correlation system such as Mott insulators. Therefore in present work, the GGA calculations are supplemented by another technique called LDA+U method[30] particularly for the low pressure regime where MnO and FeO are regarded as Mott insulators. In this LDA+U method, the strong correlation between localized d-electrons is explicitly taken into account through the screened effective electron-electron interaction parameter $U_{\rm eff}=U-J$ with U and J denoting the Coulomb and exchange integral, respectively.

Except the LDA+U calculations, the calculations for the electronic structures are performed by using the modified Car-Parrinello method.[31] The plane-wave basis pseudopotential method is used to perform the structural optimization efficiently. The $2p$-states of oxygen and $3d$-states of Mn and Fe are treated by the Vanderbilt ultrasoft pseudopotential.[32] For other states, we employ the optimized norm-conserving pseudopotentials.[33]

The cutoff energies for the wave functions $E_{\rm cut}^{\rm WF}$ and charge density expansion $E_{\rm cut}^{\rm CD}$ are 36 Ry and 200 Ry, respectively, for all calculations. Under high-pressure, there is a very short TM-O distance. Therefore small core radii have to be adopted for both TM atoms and O atoms resulting in a large cutoff energy for the wave functions. Convergence of the band structure and total energy calculations with respect to cutoff energies was carefully checked for some systems, and only negligible differences [<1 mRy/fomular unit (f.u.)] exist between the choice of 36 Ry and 30 Ry. A tetrahedron method is adopted for the k-space integration. The convergence of k-point sampling was also well checked, and the sampling of irreducible k points gives absolute total energy convergence to better than 1 mRy/f.u. Moreover, note that the convergence in the relative energy between different structures is generally order of magnitude better than the convergence in the absolute total energy. High credibility of the present approach based on the ultrasoft-pseudopotential has been well confirmed.[34] However, we should emphasize that all of our calculations are for stoichiometric materials at zero temperature. Some other parameters which have been used in our calculations are listed in Table I.

The heaviest part of the present calculations is the structure optimization for each volume and each phase. Forces acting on atoms, stress tensors[35] on unit cells and the total energies are used as guides in the structural optimization process.

TABLE I. Parameters and conditions used for present calculations. $N_{\rm s}$, $N_{\rm k}$, $E_{\rm cut}^{\rm WF}$ and $E_{\rm cut}^{\rm CD}$ mean the number of symmetry operations, the number of k points in the irreducible Brillouin zone, the cutoff energy for wave function, and the cutoff energy for charge density, respectively. ''+1'' in the third column means an additional symmetery operation used for the antiferromagnetic spin order.

	Space group	N_s	N_k	Inversion symmetry?	$E_{\rm cut}^{\rm WF}$	$E_{\rm cut}^{\rm CD}$
AF rB1	$D_{3d}^5(R\bar{3}m)$	12+1	50	yes		
FM rB1	$D_{3d}^5(R\bar{3}m)$	12	50	yes		
NM rB1	$D_{3d}^5(R\bar{3}m)$	12	50	yes		
AF B2	$D_{3d}^5(R\bar{3}m)$	12+1	33	yes		
FM B2	$D_{3d}^5(R\bar{3}m)$	12	33	yes		
NM B2	$D_{3d}^5(R\bar{3}m)$	12	33	yes	36 Ry	200 Ry
AF nB8	$D_{3d}^1(P\bar{3}1m)$	12+1	35	yes		
FM nB8	$D_{6h}^4(P6_3/mmc)$	24	30	yes		
NM nB8	$D_{6h}^4(P6_3/mmc)$	24	30	yes		
AF iB8	$C_{3h}^1(P\bar{6})$	6+1	66	no		
FM iB8	$D_{6h}^4(P6_3/mmc)$	24	30	yes		
NM iB8	$D_{6h}^4(P6_3/mmc)$	24	30	yes		

III. RESULTS AND DISCUSSION

A. Low-pressure region

1. Results based on GGA

First let us pay attention to the low-pressure region where both MnO and FeO should take the AF rB1 structure below the Néel temperature. Figure 2 shows the calculated total energies versus volume for various modifications of MnO with the B1 structure, including distorted AF rB1, undistorted AF B1, stretched NM rB1, compressed NM rB1, and FM B1 phases. For the FM B1 phase, our calculations sug-

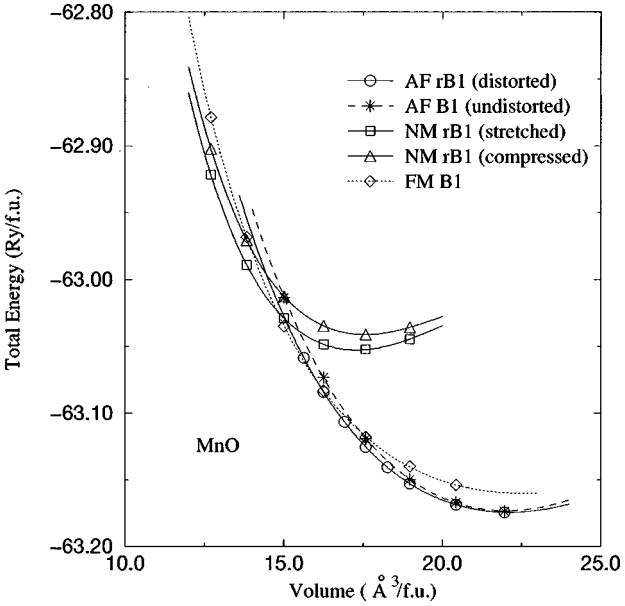

FIG. 2. The calculated total energies versus volumes for various modifications of MnO with the B1 structure. The least-squares-fitted curves to Murnaghan's equation of state are shown.

TABLE II. Equation-of-state parameters and magnetic moments of AF rB1 phases of MnO and FeO obtained by present calculations, and comparison to literatures.

	MnO		FeO	
	GGA	Expt.	GGA	Expt.
B_0 (Gpa)	157	151,[a] 162 [b]	180	142,[f] 180[g]
B'	3.23	3.6,[a] 4.8 [b]	3.55	4.9 [g]
a_0 (Å)	4.46	4.435 [c]	4.28	4.334 [f]
Moment(μ_B)	4.47	4.58,[d] 4.79 [e]	3.46	4.2 [h]

[a]Y. Noguchi *et al.*, Geophys. Res. Lett. **23**, 1469 (1996).
[b]R. Jeanloz *et al.*, J. Geophys. Res. **92**, 11 433 (1987).
[c]L. F. Mattheiss *et al.*, Phys. Rev. B **5**, 290 (1972).
[d]A. K. Cheetham and D. A. O. Hope, Phys. Rev. B **27**, 6964 (1983).
[e]D. E. F. Fender, A. J. Jacobson, and F. A. Wegwood, J. Chem. Phys. **48**, 990 (1968).
[f]C. A. McCammon *et al.*, Phys. Chem. Miner. **10**, 106 (1984).
[g]I. Jackson *et al.*, J. Geophys. Res. **95**, 21671 (1990).
[h]P. D. Battle and A. K. Cheetham, J. Phys. C **12**, 337 (1979).

gest that there will be no rhombohedral distortion. First, we can see that around the equilibrium volume at normal pressure the AF (either distorted or undistorted) state is definitely more stable than the FM and the NM states: the total energy of the NM state is much higher than that of AF state, while the FM state is energetically close to the AF state. The reasons why under normal pressure AF (with type-II) transition-metal monoxides with the B1 structure are more stable than the NM, FM, and another kind of AF (with type-I) structures have been explained in Terakura *et al.*'s early work.[36] Here we just mention simply that this is mainly because of the strong super-exchange path through oxygen. Figure 2 also shows that the rhombohedral distortion is very essensial for the stability of the AF state. If the rhombohedral distortion is absent in the AF B1 phase, the FM B1 phase may be realized with pressure beyond about 50 GPa. With increasing pressure, the difference in the total energy between the distorted and the undistorted AF B1 phases is enhanced because of the enhancement of the distortion. It can be also found that the total energy of the AF B1 phase even with rhombohedral distortion increases more rapidly than those of the FM and NM phase with increasing pressure. This implies that the FM and NM B1 phases will become more stable than the AF B1 phase at high-pressure due to the band broadening.[19] The possibility of FM and NM B1 phases as the high pressure phases of MnO will be discussed in the following part. In the case of FeO, the relative stability among different magnetic states of the B1 structure was studied by Isaak *et al.*[24] based on LDA, and our calculations based on GGA give similar results (not shown here).

By fitting the calculated energies versus volume for different phases to Murnaghan's equation of state,[37] we can determine the equation-of-state parameters (the zero pressure lattice parameter a_0, the bulk modulus B_0, and the pressure derivative of the bulk modulus B'). Our GGA results for the AF rB1 phases of both MnO and FeO are shown in Table II, together with the experimental data. Although the experimental data scatter a bit, agreement between our theoretical data and the experimental ones is fairly good.

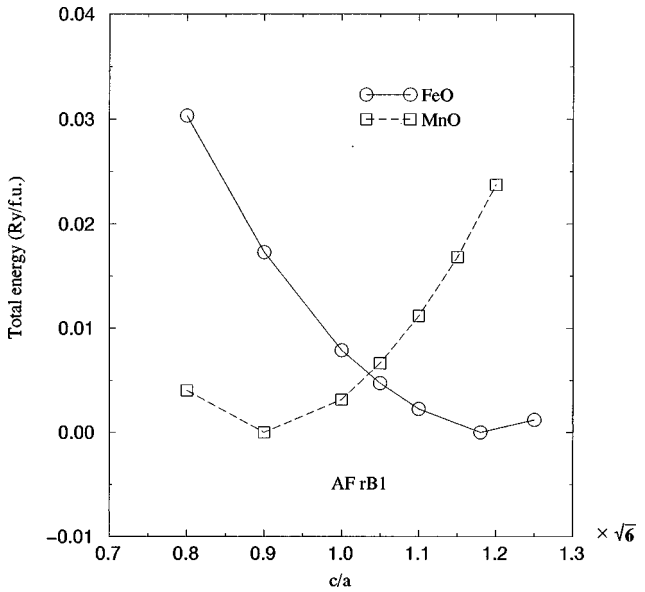

FIG. 3. The calculated total enengies of AF rB1 phases of MnO and FeO as a function of c/a ratio, where $c/a = 1.0 \times \sqrt{6}$ means no rhombohedral distortion (exactly the cubic cell). A volume ($= 18.97$ Å^3) in the low-pressure region is chosen for all calculations, and the calculated total energies are shifted so as to make the energy minima the energy origin.

As we mentioned above, the lattice distortion is very important for the AF rB1 phase. However, it is observed experimentally that for MnO and FeO the two distortions are along the opposite directions of [111] diagonal line, compressed for MnO and stretched for FeO. The present calculations based on GGA can predict the sign of this rhombohedral distortion correctly. Figure 3 shows the calculated total enengies versus c/a ratios for AF rB1 phases of MnO and FeO with a fixed volume ($= 18.97$ Å^3) in the low-pressure region, where $c/a = 1.0 \times \sqrt{6}$ means no rhombohedral distortion (exactly the cubic cell). We see clearly that the compressed structure and the stretched structure are more stable for MnO and FeO, respectively. Our calculation also shows that the two kinds of distortion will both be enhanced with increasing pressure, more compressed for MnO and more stretched for FeO, being consistent with the experimental observation.[2,4] Figure 4 shows the calculated distortions for AF rB1 phases of MnO and FeO as a function of volume. It is shown clearly that the present calculations predict correctly the tendency of the change of distortions with increasing pressure, although the distortions are overestimated. One of the possible reasons for the overestimation may be due to the fact that our calculations give the distortions at zero temperature while the experiments are performed at room temperature. Another possible reason was pointed out by two of us as originating from the overestimation of the exchange coupling constants in the level of approximations like LDA and GGA.[38]

Another interesting feature is the distortions in the NM B1 states. The NM state of FeO with the B1 structure was studied by Isaak *et al.*,[24] who found that the rhombohedral distortion exists whether the AF spin order is present or not. Similarly, our results in Fig. 5 show that the NM B1 phase of MnO is also rhombohedrally distorted. However, in contrast to the case of the AF rB1 phase (see Fig. 3) where only the

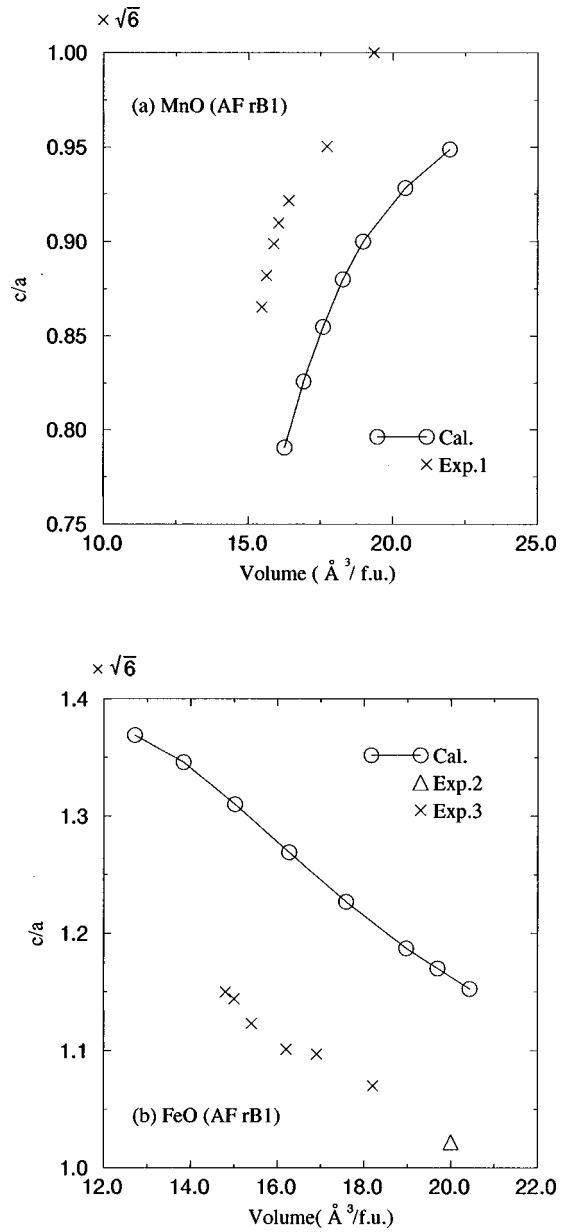

FIG. 4. The calculated rhombohedral distortion versus volume for AF rB1 phases of MnO (a) and FeO (b), and comparison with experimental results. Exp.1, Exp. 2, and Exp. 3 come from Refs. 2–4, respectively.

compressed rhombohedral distortion is stable, both the compressed and stretched modes are locally stable in the NM B1 phase and moreover the stretched one is more stable. Therefore, if the magnetic phase transition from AF to NM state may be realized for MnO by pressure, the rhombohedral distortion has to switch from the compressed mode to the stretched mode. On the other hand for FeO, the stretched mode is more stable both in AF and NM B1 states.

In contrast to all the success of GGA shown above, there exists a problem related to the AF rB1 phases of both MnO and FeO: the GGA is not powerful enough to describe the band gaps of Mott inuslators correctly. The calculated DOSs for MnO and FeO with the AF rB1 phase are shown in Figs. 6(a) and 6(b). A volume ($=18.97$ Å^3) close to the equilibrium value is chosen. For MnO, the states from -0.7 to -0.3 Ry are predominantly O $2p$-states, and those from -0.3 Ry

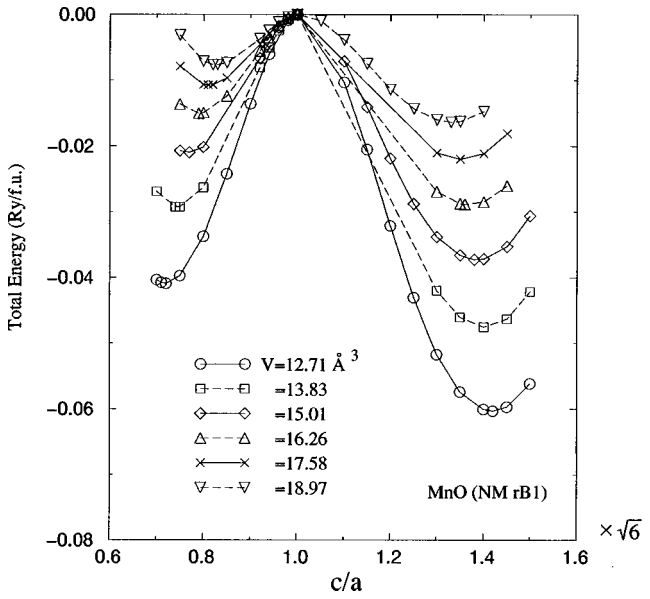

FIG. 5. The calculated total energies versus rhombohedral distortion c/a for different volumes of NM rB1 MnO. The energies for the lattices with no distortion are taken to the energy origin.

to Fermi level E_F are mostly Mn $3d$. Because of the half-filled d band in MnO, the GGA can make it insulating [Fig. 6(a)] and the compressed rhombohedral distortion enhances the band gap. Nevertheless, the obtained band gap is much too small compared with the experimental value of 3.9 eV.[39] A possible problem of GGA in the relative stability among different phases of MnO will be discussed in the following part. In contrast to MnO, because of the additional electron in the minority-spin Fe $3d$ band, GGA makes FeO metallic

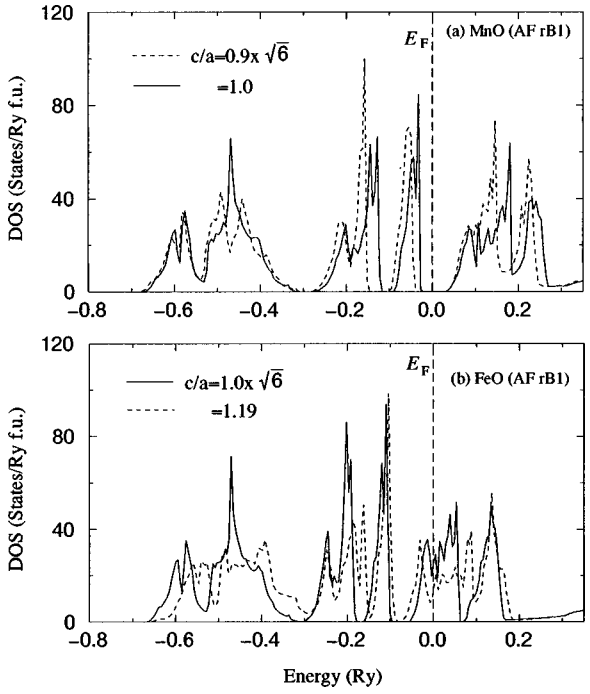

FIG. 6. The calculated total DOS curves for AF rB1 phases of MnO (a) and FeO (b) with different c/a ratios. A volume ($=18.97$ Å^3) close to the equilibrium volume is chosen for the calculations.

[see Fig. 6(b)]. The GGA is not sufficient to split the Fe t_{2g} bands, although the streched rhombohedral distortion will reduce the DOS at the Fermi level E_F. The failure of GGA in describing the electronic structure of AF rB1 FeO causes incorrectly stronger stability of the AF iB8 phase compared with the AF rB1 phase at normal pressure.[29] It was pointed out that this inconvenient aspect can be removed by the LDA+U method with the SOC taken into account. As the proper description of the ground state of FeO requires careful treatment of several ingredients such as electron correlation, SOC and lattice distortion, we present detailed analysis of the electronic and magnetic properties of FeO in the next subsection.

2. Ground state properties of FeO at normal pressure

In the ordinary band-structure calculation, the ground state of FeO with the cubic crystal has one electron in the triply degenerate t_{2g} orbitals in the minority spin band. In order to make FeO insulating, population imbalance among the minority-spin t_{2g} orbitals has to be induced. The type-II AF ordering and rhombohedral lattice distortion produces trigonal symmetry to lift the triple degeneracy of the t_{2g} orbitals, leading to partial population imbalance. However, the present GGA calculation suggests that these origins of symmetry breaking are not strong enough to make FeO insulating. Another important origin of population imbalance is the Coulomb interaction among t_{2g} electrons. In addition to these factors, we have to take into account the SOC which is known to play an important role in the t_{2g} manifold.[40] The SOC, can determine the easy axis for spin magnetic moments and then determine a particulat linear combination of the t_{2g} orbitals to be preferentially occupied, producing orbital magnetic moment.

These problems were first discussed by Kanamori.[40] The magnetocrystalline anisotropy energy (E_{MA}) in the rB1 phase consists of the cubic (K) and the trigonal (T) terms:[40]

$$E_{MA}=K\{e_x^2e_y^2+e_y^2e_z^2+e_z^2e_x^2\}+T\{e_xe_y+e_ye_z+e_ze_x\}, \tag{1}$$

where $\{e_i\}$ are the direction cosines of the spin magnetic moments referred to the ideal rock-salt cell. Even with this simplified model one can expect (see Appendix) a rather rich phase diagram for the directions $\{e_i\}$. Combination of different signs and the relative strength of K and T can result in various scenarios of the equilibrium such as the easy [111] and [001] axes, the easy (111) plane as well as the wide spectrum of solutions where the magnetic moments cant off the high symmetry directions (Fig. 7).

The cubic anisotropy K is the fourth order effect with respect to SOC, whereas the trigonal anisotropy T appears in the (lowest) second order. Since the majority-spin Fe $3d$ states are almost fully occupied in the low-pressure AF B1 phase of FeO, the SOC affects mainly the minority-spin channel. Then, the trigonal anisotropy energy is directly related with the magnitude of the orbital angular momentum, and the easy magnetization direction should be such that the orbital moment is least quenched when the magnetization is directed along the particular direction (see, e.g., discussions by Bruno[41]). The type-II AF spin order and the rhombohedral lattice distortion will split the atomic minority-spin Fe

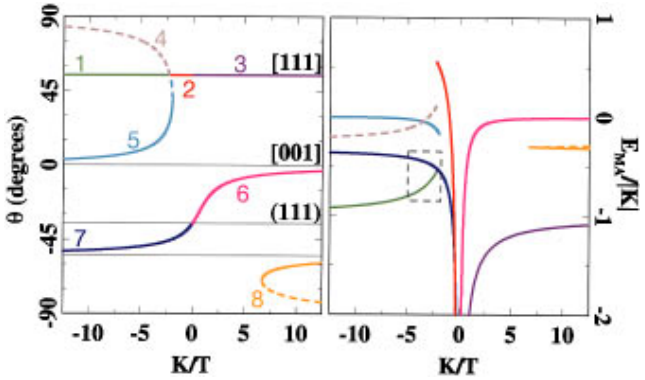

FIG. 7. (Color) Left panel: angle between the magnetic easy axis in the $(1\bar{1}0)$ plane and [001] direction of the cube depending on the signs and relative strength of the cubic (K) and trigonal (T) anisotropies. $K<0$ $T<0$ (branches 3 and 8); $K<0$ $T>0$ (branches 1, 4, 7); $K>0$ $T<0$ (branches 2, 5); $K>0$ $T>0$ (a branch 6). Parts of the diagram corresponding to an unstable equilibrium are shown by broken lines. The angles corresponding to the characteristic [111] and [001] directions of the cube as well as the plane (111) are marked by the labels. Right panel: corresponding magnetic anisotropy energy.

t_{2g} states in two subgroups corresponding to the one-dimensional a_{1g} representation

$$|a_{1g}\rangle=\frac{1}{\sqrt{3}}(|xy\rangle+|yz\rangle+|zx\rangle)$$

and the two-dimensional e_g representation

$$|e_g^1\rangle=\frac{1}{\sqrt{6}}(2|xy\rangle-|yz\rangle-|zx\rangle),$$

$$|e_g^2\rangle=\frac{1}{\sqrt{2}}(|yz\rangle-|zx\rangle).$$

If the degenerate e_g representation corresponds to the lower energy, the largest ($1\mu_B$) orbital moment can be obtained if it is aligned parallel to the [111] direction and the occupied e_g orbital is $(1/\sqrt{2})(|e_g^1\rangle+i|e_g^2\rangle)$. In the case of reverse order of the atomic levels when the a_{1g} representation is energetically more favorable, the Cartesian components of the angular momentum are given by the regular perturbation theory expansion in the first order of the SOC ξ as $\langle\hat{L}_k\rangle=(\xi/3\Delta_{rh})(2e_k-e_l-e_m)$, where Δ_{rh} is the energy splitting between the a_{1g} and the e_g representations, and (klm) is an even permutation of (xyz). Thus, the orbital moment is totally quenched along the [111] direction and unquenched in the (111) plane. Thus, the stabilization of the a_{1g} representation would lead to an in-plane magnetic alignment.

Below we summarize results of our ASA-LMTO LDA+U calculations[42] performed in this context.

First, we consider the case without the rhombohedral distortion when the AF spin order is the only factor which could determine the a_{1g}-e_g splitting among the t_{2g} states. Even without the SOC, depending on the starting Fe $3d$-configuration, we were able to obtain two different types of self-consistent LDA+U solutions: the occupied minority-

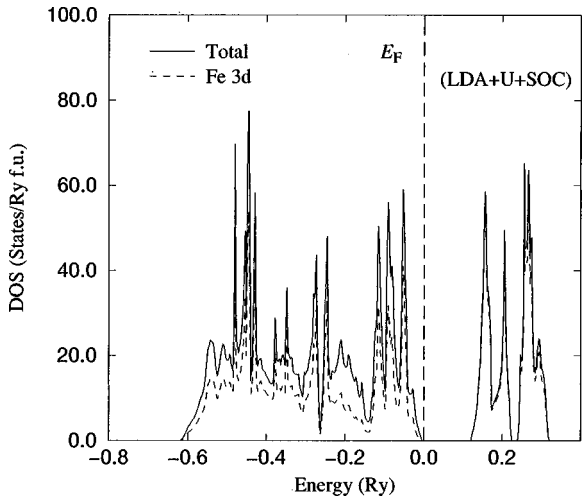

FIG. 8. Total DOS and projected DOS onto Fe 3*d* orbital of AF rB1 FeO by using LDA+*U* method with SOC taken into account. The calculation is performed for a volume=18.97 Å^3 with optimized c/a.

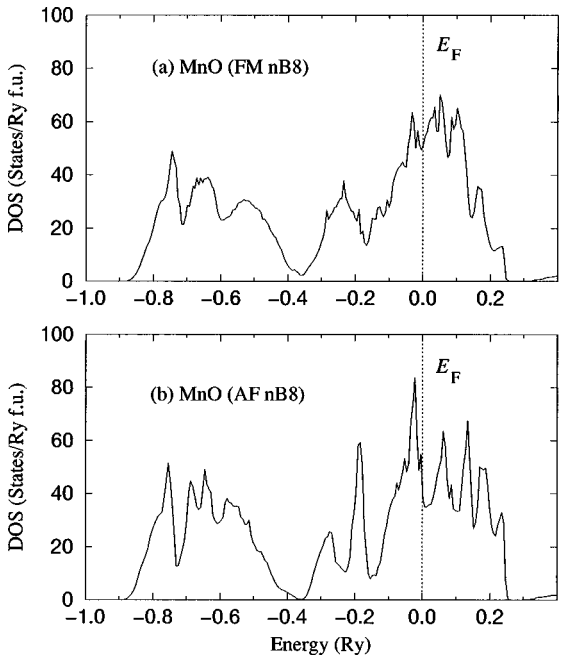

FIG. 9. The calculated total DOS curves for FM (a) and AF nB8 (b) phases of MnO for the volume (=13.83 Å) corresponding to the pressure about 120 GPa.

spin t_{2g} states were mainly of either (*a*) a_{1g} character or (*b*) e_g character. Thus, the AF spin order alone does not define unambiguously the sign of the trigonal splitting and the two obtained solutions correspond to the scenarios when the symmetry of the triply-degenerate t_{2g} shell is spontaneously broken by U_{eff}. After including the SOC, the solution (*a*) leads to the canted spin state belonging to the branch 7 in Fig. 7 (i.e., the situation effectively corresponds to $K<0$ and $T>0$). Once the gap in the minority-spin t_{2g} band is opened by U_{eff}, the solution (*a*) becomes rather insensitive to the choice of the LDA+U parameters. For example, when U_{eff} varies from 4.0 to 7.0 eV, the orbital moment at Fe site varies only from 1.096 to 1.105 μ_B, and the canting angle in the $(1\bar{1}0)$ plane $\theta=\arcsin(\sqrt{2}e_x)$ varies only from -46.7 to -47.4 degrees. Note that the confinement of the spin magnetic moments in the $(1\bar{1}0)$ plane does not destroy the generality of the argument based on Eq. (1). The solution (*b*) leads to the easy [111] axis scenario, also accompanied by the large orbital magnetic moment (1.088 μ_B for $U_{\text{eff}}=7$ eV).

The situation is however different when the rhombohedral distortion $c/a=(1+\delta)\times\sqrt{6}$ is taken into account. The case of $\delta=\pm 0.15$ was considered in our previous work.[43] Here we just summarize the main results. Even for these moderate distortions (see the scale in Fig. 3), the trigonal anisotropy becomes dominating $|T|\gg|K|$. The sign of $|T|$ is determined by the direction of the distortion as $\text{sign}(T)=-\text{sign}(\delta)$. Then, the stretching $\delta>0$ and the compression $\delta<0$ will stabilize the magnetic moments parallel to the [111] axis and the (111) plane, respectively. Thus, the rhombohedral distortion is a very important factor which determines the equilibrium magnetic structure in the rB1 AF phase of FeO. However, the existence of the rhombohedral instability already in the NM rB1 state[24] suggests that the origin of the distortion itself and its direction $\delta>0$ may not be directly related with the magnetism of FeO. The stretching mode $\delta>0$ in FeO (Fig. 3) corresponds to the easy [111] axis scenario, which is accompanied by the orbital magnetization of nearly 1 μ_B.[43]

For the optimized δ and after including U_{eff} and SOC, the DOS of AF rB1 FeO is shown in Fig. 8.

B. High-pressure phases

1. MnO

As already mentioned, the high-pressure phase of MnO has been expected to be the B2 structure. For different magnetic states of B2 structure, our calculations show that the AF state always have definitely lower energies than the FM and NM states within the whole volume range of our calculations. With increasing pressure, the AF B2 structure will become more stable than the AF rB1 structure.[29] However, it is also shown by our calculations that at about 120 GPa the nB8 structures will be more than 10 mRy/f.u. more stable than the AF B2 phases. Actually the nB8 structures are the most stable high-pressure phase of MnO rather than B2 structure.[29] Detailed comparison of the total energies for the FM and AF ordering nB8 structures predicts that the FM and AF states of the nB8 structure are nearly degenerate in energy under high pressure. The calculated electronic densities of states (DOS) for the FM and AF nB8 phases of MnO with volume 13.83 Å/f.u., which corresponds to about 120 GPa, are shown in Fig. 9, where the states from -0.9 to -0.4 Ry are mostly O $2p$ states and those above -0.4 Ry are mostly Mn $3d$ states. Definitely these two DOSs are almost the same except with some marginal differences. This degeneracy is mostly because of the reduction of magnetic moment under high-pressure (see Fig. 14).

From our calculations, a first-order phase transition is expected to occur from the insulating AF rB1 structure to the metallic nB8 structure. This can be seen more clearly from Fig. 10, which gives the calculated enthalpy of different phases as a function of pressure. The cross points of these enthalpy-pressure curves give the phase-transition critical

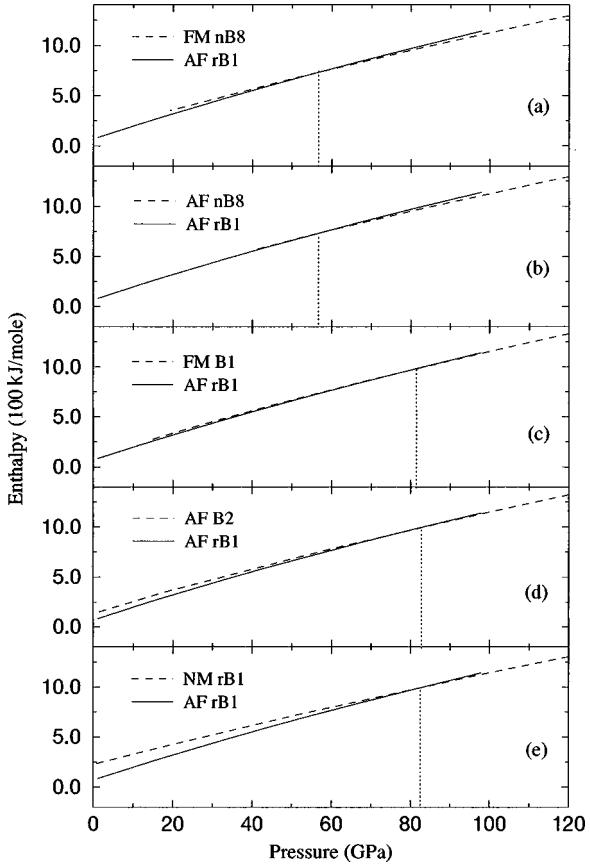

FIG. 10. Calculated enthalpy against pressure for different phases of MnO. Transitions from AF rB1 to (a) FM nB8; (b) AF nB8; (c) FM B1; (d) AF B2; (e) NM rB1 are shown.

pressures. This prediction can explain the recent experiment[2] on MnO in a high pressure range (>120 GPa) very well. For example, if we assign the experimental x-ray diffraction peaks at 137 GPa by the nB8 structure, almost an exact fit of peak positions and good agreement of the intensity profile can be obtained except one peak for $d_{\mathrm{exp}}=1.844$ Å which is analyzed to originate from the metastable NM rB1 phase (as discussed below). The intensity of this peak is actually reduced after annealing.

However, the critical pressure for the first-order transition from the AF rB1 structure to the nB8 structure (either FM or AF state) is estimated to be about 60 GPa [see Figs. 10(a) and 10(b)], which is much lower than the experimental transition pressure. We suggest two possibilities to interpret this discrepancy. First, as already discussed above, transition-metal monoxides are strongly correlated electron systems and even GGA is not sufficient to describe properly their electronic structure particularly in the low pressure region. This implies that the real energy-volume curve of the insulating AF rB1 structure should be lower than the calculated one using GGA due to the underestimation of the band gap. This will lead to a higher critical pressure. To check this possibility, we performed supplementary LDA+U calculations, which have been regarded as one way to treat the system with strong correlation. By performing the LDA+U calculation with the plane-wave basis pseudopotential method for one fixed volume ($=17.58$ Å^3) in the low pressure range with a reasonable choice of parameter U_{eff}

TABLE III. Comparison of the results between GGA and LDA+U calculations for MnO with a fixed volume ($=17.58$ Å^3) in the low pressure region. The total energy differences between the AF rB1 phase and other phases are shown in units of mRy/f.u.

	GGA	LDA+U
$E_{(\mathrm{FM\ B1})}-E_{(\mathrm{AF\ rB1})}$	7.418	15.146
$E_{(\mathrm{AF\ B2})}-E_{(\mathrm{AF\ rB1})}$	22.254	31.234
$E_{(\mathrm{AF\ nB8})}-E_{(\mathrm{AF\ rB1})}$	3.836	14.304
$E_{(\mathrm{FM\ nB8})}-E_{(\mathrm{AF\ rB1})}$	13.410	46.722

$=4.0$ eV, we obtained the results shown in Table III. Indeed we see that the stability of the insulating AF rB1 structure relative to all other phases (including FM B1, AF nB8, FM nB8, and AF B2) is enhanced compared with the GGA results. The second possibility is that the transition barrier from the rB1 to nB8 structure may be fairly high because of the significant rearrangement of the atom position. The existence of this transition barrier will generally make the actual transition pressure higher than the calculated one.

Figure 11 shows the pressure-volume (P-V) relation for MnO obtained by the present calculation and also by experiments. In order to avoid confusion, only important phases are presented here. Clearly, in the low pressure range, the sample is in the AF rB1 phase, and the calculated P-V curve is in good agreement with the experimental results. On the other hand, the highest pressure data point obtained by the static compression followed by laser annealing is just on the line of the P-V curve for the nB8 structure. We estimated the tem-

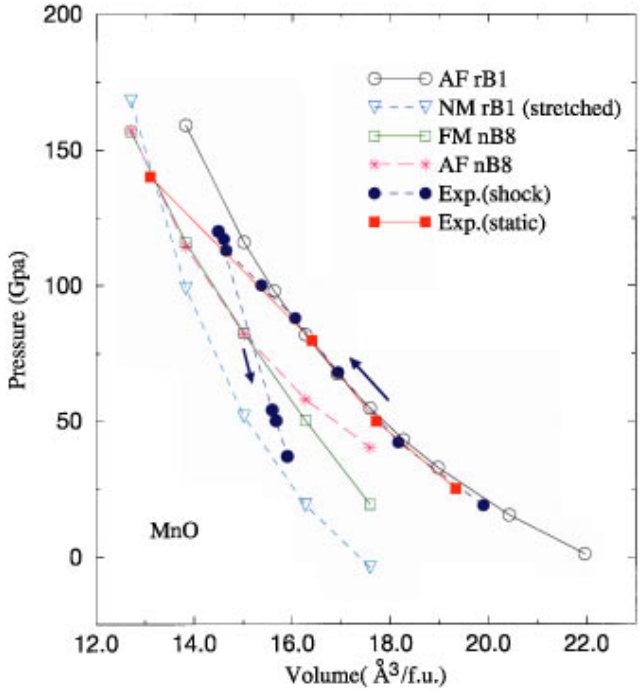

FIG. 11. (Color) The calculated pressure-volume curves for different phases of MnO, and comparison with experimental results. Two experimental results with shock compression (Ref. 5) and static compression (Ref. 2) (at room temperature) are shown, and the experimental data for decompression process in the shock compression experiment are also shown. The arrows indicate the process of the shock experiment.

perature effect on the P-V relation by the experimental data on the AF rB1 phase of MnO. We found that generally the temperature around 1000 K will cause a pressure change of about a few percent with respect to the pressure at 0 K.

Experimentally the high-pressure nB8 phase of MnO seems not to be realized directly from the low-pressure AF rB1 phase because of the high transition energy barrier. There may exist some intermediate-pressure phases.[2] The experimental x-ray diffraction pattern in the intermediate pressure range (90–120 GPa) cannot be explained simply by a single phase. The shock compression experimental data point around 120 GPa for the pressure-volume relation is located just in between the curves corresponding to the AF rB1 and FM or AF nB8 structures, suggesting that the sample is in a mixed phase. Even in the high-pressure region (>120 GPa), there is an additional x-ray peak not coming from the nB8 structure. All these situations suggest that MnO may undergo some complicated phase transition paths in the intermediate pressure region between the normal-pressure insulating AF rB1 phase and the high-pressure metallic nB8 phase.

The present results shown in Fig. 10 suggest three possible transitions from the AF rB1 phase: (1) to the FM B1 phase, (2) to the AF B2 phase, and (3) to the NM rB1 phase. All these three transitions have similar critical transition pressure of about 80 GPa. We should note that the B2 structure is a special case of the rB1 structure with $c/a=0.5\times\sqrt{6}$. Therefore the transition (1) and (2) in the above may be kinematically easy to occur because only the change in the c/a is required. However, the x-ray diffraction pattern in the intermediate pressure range can be explained by neither the FM B1 phase nor the AF B2 phase.

We would like to point out that the NM rB1 phase is actually realized in the intermediate pressure range and that it persists even at the highest pressure (137 GPa) attained by the experiment. It was mentioned in the preceding section that the sharp peak corresponding to $d_{\mathrm{exp}}=1.844$ Å cannot be assigned as originating from the AF or FM nB8 structure. The peak can be assigned as (102) reflection of the NM rB1 structure. We performed simulation of the x-ray diffraction pattern corresponding to the NM rB1 structure at 137 GPa. Very interestingly, most of the other peaks of the NM rB1 structure nearly overlap with the peaks coming from the AF or FM nB8 structure. The observed broad peaks may be partly caused by the superposition of the peaks of two structures. However, as was mentioned earlier, the peaks originating from the NM rB1 structure diminish by laser annealing implying that the NM rB1 structure is metastable under pressure as high as 137 GPa. Some of the x-ray peaks in the intermediate-pressure range (90–120 GPa) can be assigned as originating from the NM rB1 structure too.

The shock compression experiment only reaches the pressure of about 120 GPa. This suggests that the high pressure phase observed by the shock compression experiment may be more populated by the NM rB1 structure. This assignment may be supported by an additional aspect. The pressure-volume curve in the decompression process obtained by the shock experiment (see Fig. 11) indicates that their high-pressure phase has a very much reduced volume at the pressure as low as about 40 GPa. Further lowering of the pressure cannot keep the sample in the high-pressure phase. The present calculation suggests that only the NM rB1 structure can have such a reduced volume and the calculated pressure-volume curve seems to agree with the experimental data for the decompression process.

2. FeO

The calculations for FeO are similar. Surprisingly, we find that the iB8 structure with the AF ordering is the most stable phase among several structures.[29] Here we want to discuss in more detail why the nB8 structure is realized for most of the transition-metal compounds with the B8 structure, while the iB8 structure is uniquely so stable as the high-pressure phase of FeO.

In the nB8 structure, a transition metal ion is coordinated by anions octahedarally, while anions around a transition metal in the iB8 structure form a trigonal prism (see Fig. 1). Apparently, the TM site is an inversion center in the former and not so in the latter. As to the oxygen site, it is not an inversion center in the nB8 structure irrespective of the magnetic order on the TM site. On the other hand, whether the oxygen site in the iB8 structure is an inversion center or not depends on the magnetic order on the TM site: the oxygen site is an inversion center in the FM order and not so in the AF order. Consequently, an inversion center does not exist in the AF iB8 structure and does exist in the AF nB8 structure. Absence of the inversion symmetry reduces the strength of the hybridization of the $3d$-orbitals with the oxygen $2p$-orbitals. Such a reduction in the p-d hybridization in the iB8 structure compared with that in the nB8 structure was confirmed in the present calculation by estimating the energy separation between the centers of the p- and d-bands. For example, for a significantly compressed volume ($=14.84$ Å^3) with fixed $c/a=2.0$ for both AF nB8 and AF iB8 FeO, the $p-d$ band-center energy separation of AF nB8 phase is about 0.12 eV larger than that of AF iB8 phase. As the p-d hybridization contributes to the stability of the structure, this aspect favors the nB8 structure and will explain the general feature that the nB8 structure is actually realized in most cases. In order to understand any reason for the special situation of FeO, we calculated the DOSs for both nB8 and iB8 with different magnetic structures. It is found that the combination of AF and iB8 is very unique in the sense that the electronic structure is insulating. In order to make the situation clearer, Fig. 12 gives the calculated partial densities of states for Fe $3d$-orbitals in FeO with AF iB8 structure. We can see clearly that a well defined band gap exists at the Fermi level. For this AF iB8 structure the majority spin band is completely occupied and only one subband is occupied in the minority spin state to accommodate additional one electron because Fe^{2+} has a $d_{\uparrow}^{5}d_{\downarrow}^{1}$ electron configuration. This occupied subband of minority spin state has a mixed character of $3z^2-r^2$, x^2-y^2, and xy orbitals, all of which hybridize with the oxygen $2p$-orbitals only weakly. Note that the z axis is along the crystal c axis. Appearance of the band gap at the Fermi level will contribute to special stability of this AF iB8 structure. It should be noted that the AF iB8 FeO is a band insulator rather than a Mott insulator because it is insulating even in the high pressure range where the Mott insulating condition breakes down.[19,44] The calculated band gap even increases slightly with pressure: 0.05 Ry at normal

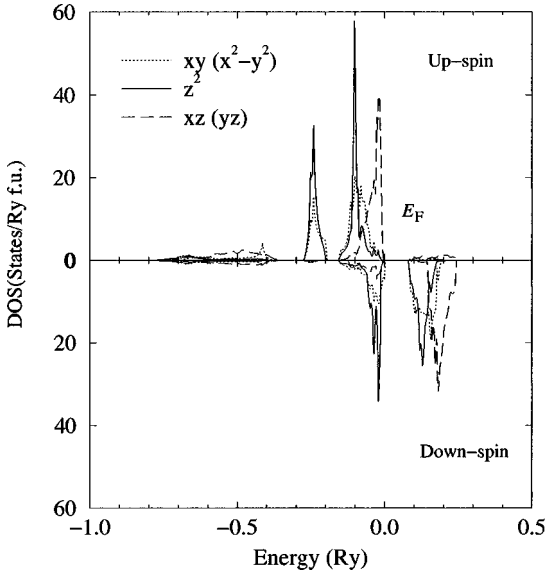

FIG. 12. The partial densities of states for Fe *d* orbitals in FeO with AF iB8 phase.

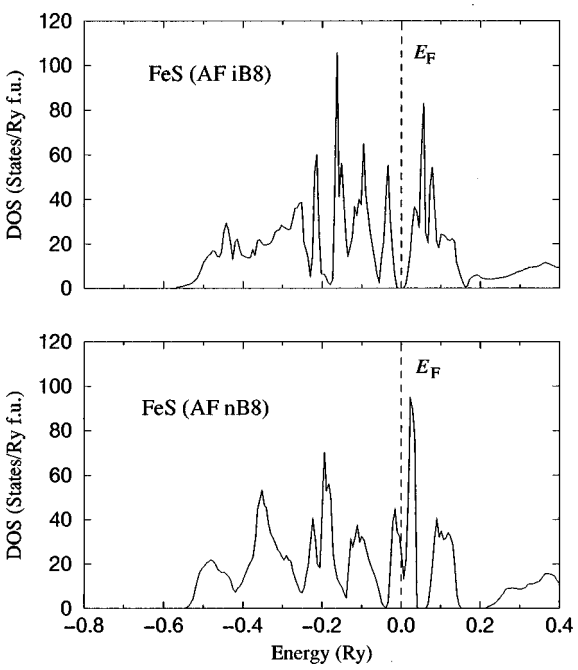

FIG. 13. The DOS curves for FeS with the optimized structures of AF iB8 and AF nB8 phases, respectively.

pressure and 0.07 Ry at 96 GPa. Such a behavior will not be expected for Mott insulators.

The uniqueness of FeO may become even clearer by comparing FeS with FeO because S is right below O in the Periodic Table. Although the real crystal structure of FeS is not exactly the B8 structure, it can be regarded as a superstructure based on B8 and it is basically the nB8 structure rather than the iB8 structure. The aim of these calculations is not to discuss the stability of the real crystal structure of FeS but to study the relative stability of the nB8 and iB8 structures for FeS. In the calculation, the unit cell volume is fixed as the experimental equilibrium value[45] under normal pressure and the c/a ratio is optimized for each of the nB8 and iB8 structures. The total energy calculations predict that the nB8 structure is more stable than the iB8 structure for FeS by 11.7 mRy/f.u. The theoretical value of the c/a ratio for the AF nB8 phase of FeS is 1.65 being in good agreement with the experimental one ($=1.71$), while the optimized c/a for AF iB8 structure is 1.98. The DOS curves for FeS with nB8 and iB8 structures are shown in Fig 13, where the states from -0.6 to -0.24 Ry are mostly S $3p$-states and those above -0.24 Ry are mostly Fe $3d$-states. The AF iB8 phase of FeS also has a band gap. However, the band gap of only about 0.01 Ry is not large enough to stabilize the AF iB8 phase.

IV. SUPPLEMENTARY DISCUSSIONS

A. Magnetic moment

The magnetic moment of the TMMO system is also very important especially for the study of high-pressure phases, because of the possible collapse of magnetic moment under high-pressure. However, the magnitude of magnetic moment in the AF compound cannot be determined unambiguously. It depends on the cutoff sphere radius around the magnetic ion. In the present calculation the sphere around the TM atom is chosen so as to make the magnetic moment maximal with respect to the sphere radius. For example, at the equilibrium volume of the AF rB1 structure, the sphere radii determined this way are 2.4 Å and 2.2 Å for MnO and FeO, respectively. The magnetic moment defined within the sphere is given in Table II. The discrepancy between theory and experiment for MnO was discussed recently by two of the present authors.[38] The experimental value for FeO was estimated from the neutron diffraction data by considering the Fe deficiency problem in nonstoichiometric $Fe_{1-x}O$. A qualitative agreement between the theory and and experiment can be found, if we consider about $1\mu_B$ contribution of orbital moment (see Sec. III A 2 and also Ref. 43).

Moreover, our calculated magnetic moment at TM site as a function of volume for different phases of MnO and FeO is shown in Fig. 14. We can see clearly that for all of the phases the magnetic moments will decrease with the increase of pressure. For the AF rB1 phase of MnO, we can obtain definitely two stable states, the high-spin state and the low-spin state. As discussed above, the high-spin to low-spin transition for AF rB1 phase of MnO can be realized in the intermediate-pressure range. Appearance of a kink for the FM nB8 phase of MnO also suggests the possible existence of a high-spin to low-spin transition for the FM nB8 MnO at about 120 GPa, consequently causing the sudden change of the c/a ratio. However, for the AF nB8 phase of MnO and for all of the phases of FeO, no sharp high-spin to low-spin transition has been found in the pressure range of our calculation.

B. *c/a*

We would like to make a brief comment on the c/a values of the nB8 structure of MnO and the iB8 structure of FeO as shown in Fig. 15. In the high-pressure phases, the c/a value of both systems exceeds 2.0, being unusually large compared with the values for most of the other related systems, which generally have a c/a value close to the ideal value ($c/a = \sqrt{8/3}$) for the close-packed structure. However, we have found that c/a is an increasing function of r_c/r_a with

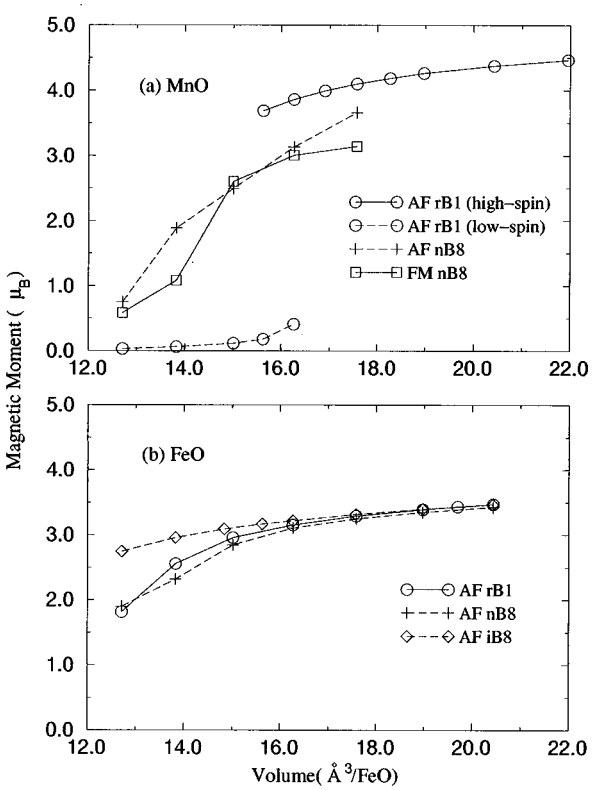

FIG. 14. The calculated magnetic moments at TM sites as a function of volume for different phases of MnO (a) and FeO (b).

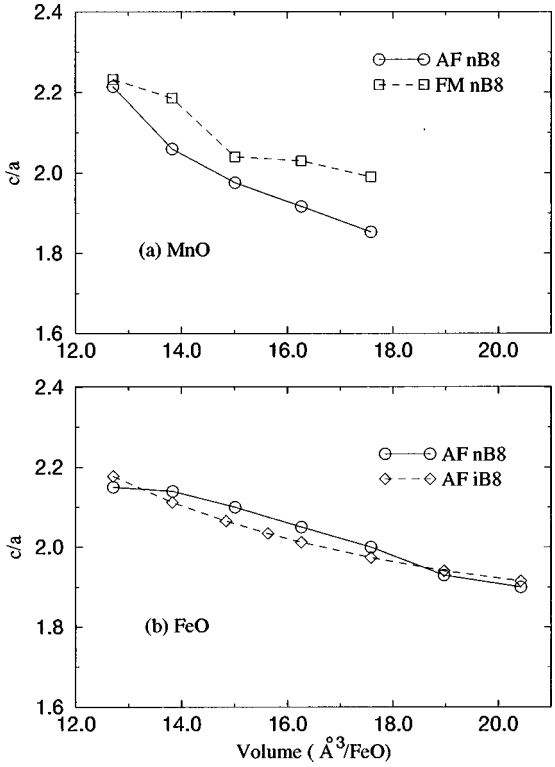

FIG. 15. The optimized c/a ratios versus volumes for different phases of MnO (a) and FeO (b).

r_c (r_a) denoting the cation (anion) ionic radius. This can be seen clearly from Fig. 16, which gives the c/a value of different materials under ambient condition as a function of cation/anion ratio. All of these materials take basically the nB8 structure at normal pressure and room temperature. Our calculations suggest that both the nB8 structure for MnO and the iB8 structure for FeO have c/a values less than 2.0 at normal pressure. This c/a value is not so unusual, because it is well on the extrapolated line of the general trend. With increase of pressure, the r_c/r_a ratio will increase due to the decrease of charge-transfer. Consequently, the c/a value for both nB8 MnO and iB8 FeO will increase to become larger than 2.0 at high pressure.

V. SUMMARY OF RESULTS

The high-pressure electronic structures and the phase stability of transition metal monoxides MnO and FeO under high-pressure were studied systematically by performing the first-principles plane-wave basis pseudopotential calculations based on DFT. Results of highly converged total energy calculations were presented for different crystal structures (B1, B2, nB8, and iB8) with different spin structures (AF, FM and NM). The electron correlation was treated by the GGA and supplemented by LDA+U method. The present calculations account well for the properties of MnO and FeO especially in the high-pressure region. The calculated equation-of-state parameters and the predicted structure distortions of different phases are in good agreement with experimental results, except the band gap problem. Our results predict that the high-pressure phase of MnO should take the nB8 structure rather than the B2 structure. In the intermediate-pressure range for MnO, the NM rB1 phase with streched distortion can be realized. A very unique AF iB8 structure rather than the nB8 structure is predicted as the high-pressure phase of FeO. This AF iB8 structure should be a band insulator even under high-pressure. The uniqueness of AF iB8 structures as the high pressure phase of FeO was further emphasized by comparing

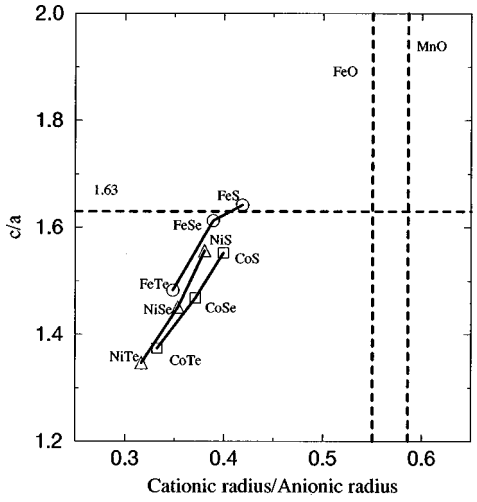

FIG. 16. The c/a value versus ionic radius ratio r_c/r_a (r_c: cation radius; r_a: anion radius) for different materials, which take the nB8 structure, under ambient condition. The ionic radii of Shannon and Prewitt (Ref. 46) are used, and the data for the c/a values come from Ref. 47. The $c/a=(\sqrt{\frac{8}{3}})\approx 1.63$ is the ideal value for the close-packed structure. The vertical lines correspond to r_c/r_a values for FeO and MnO at zero pressure.

it with the FeS case. Finally, the large c/a ratios for both nB8 MnO and iB8 FeO can be explained based on the analysis of the cation-radius/anion-radius ratio versus c/a for series of related materials.

ACKNOWLEDGMENTS

The authors thank Professor Y. Syono, Professor T. Yagi, Y. Noguchi, and Dr. T. Kondo for many valuable comments and for providing us with their experimental data before publication. Thanks are also due to Dr. Y. Morikawa and Dr. T. Miyazaki for giving us much help on computation. The present work was partly supported by New Energy and Industrial Technology Development Organization (NEDO) and also by the Grant-in-Aid for Scientific Research from the Ministry of Education, Science and Culture of Japan.

APPENDIX A: MODEL FOR MAGNETOCRYSTALLINE ANISOTROPY ENERGY IN B1 PHASE

Let us turn to the new coordinate system in which the x and y axes are rotated about the z axis by 45° in the ideal rock-salt structure. The transformation for the direction cosines is given by

$$\begin{pmatrix} e_x \\ e_y \end{pmatrix} = \frac{1}{\sqrt{2}} \begin{pmatrix} -\widetilde{e_x}+\widetilde{e_y} \\ \widetilde{e_x}+\widetilde{e_y} \end{pmatrix}. \tag{A1}$$

Then, taking into account that $e_z=(1-e_x^2-e_y^2)^{1/2}$, Eq. (1) can be transformed to

$$E_{\mathrm{MA}}=\frac{K}{4}\{4\tilde{e}_x^2+4\tilde{e}_y^2-10\tilde{e}_x^2\tilde{e}_y^2-3\tilde{e}_x^4-3\tilde{e}_y^4\} + \frac{T}{2}\{\tilde{e}_y^2-\tilde{e}_x^2+2\sqrt{2}(1-\tilde{e}_x^2-\tilde{e}_y^2)^{1/2}\}. \tag{A2}$$

Two equilibrium conditions $\partial E_{\mathrm{MA}}/\partial\tilde{e}_x=0$ and $\partial E_{\mathrm{MA}}/\partial\tilde{e}_y=0$ yield

$$K\{2-5\tilde{e}_y^2-3\tilde{e}_x^2\}\tilde{e}_x-T\left\{1+\sqrt{2}\frac{\tilde{e}_y}{(1-\tilde{e}_x^2-\tilde{e}_y^2)^{1/2}}\right\}\tilde{e}_x=0 \tag{A3}$$

and

$$K\{2-5\tilde{e}_x^2-3\tilde{e}_y^2\}\tilde{e}_y+T\left\{\tilde{e}_y+\sqrt{2}\frac{1-\tilde{e}_x^2-2\tilde{e}_y^2}{(1-\tilde{e}_x^2-\tilde{e}_y^2)^{1/2}}\right\}=0, \tag{A4}$$

respectively. Then, we consider only those solutions where the spin magnetic moments are confined within the $(1\bar{1}0)$ plane and, therefore, $\tilde{e}_x=0$. Then, Eq. (A3) is fulfilled automatically, and Eq. (A4) leads to the equilibrium condition for $\tilde{e}_y$:

$$\frac{\tilde{e}_y+\sqrt{2}\dfrac{1-2\tilde{e}_y^2}{(1-\tilde{e}_y^2)^{1/2}}}{\tilde{e}_y(2-3\tilde{e}_y^2)}=-\frac{K}{T}. \tag{A5}$$

The solution of Eq. (A5) corresponds to the minimum of E_{MA} if $\partial^2 E_{\mathrm{MA}}/\partial\tilde{e}_x^2|_{\tilde{e}_x=0}>0$ and $\partial^2 E_{\mathrm{MA}}/\partial\tilde{e}_y^2|_{\tilde{e}_x=0}>0$, which additionally lead to the requirements:

$$K\{2-5\tilde{e}_y^2\}-T\left\{1+\frac{\sqrt{2}\tilde{e}_y}{(1-\tilde{e}_y^2)^{1/2}}\right\}>0 \tag{A6}$$

and

$$K\{2-9\tilde{e}_y^2\}+T\left\{1-\sqrt{2}\tilde{e}_y\frac{3-2\tilde{e}_y^2}{(1-\tilde{e}_y^2)^{3/2}}\right\}>0. \tag{A7}$$

If one of the conditions (A6),(A7) is not fulfilled, the equilibrium is unstable. The corresponding phase diagram is shown in Fig. 7.

*Present address: Nippon Steel Corporation, Advanced Technology Research Laboratories, 3-35-1 Ida, Nakahara-ku, Kawasaki 211-0035, Japan.

[1] N. F. Mott, *Metal-insulator Transitions* (Taylor & Francis Ltd., London, 1974).

[2] T. Yagi, T. Kondo, and Y. Syono, in *Shock Compression of Condensed Matter*, edited by S. C. Schmidt *et al.* (AIP Press, New York, 1998); T. Kondo, T. Yagi, Y. Syono, T. Kikegawa, and O. Shimomura, Rev. High Pressure Sci. Technol. **7**, 148 (1998).

[3] B. T. M. Willis and H. P. Rooksby, Acta Crystallogr. **6**, 827 (1953).

[4] T. Yagi, T. Suzuki, and S. Akimoto, J. Geophys. Res. **90**, 8784 (1985).

[5] Y. Syono, Y. Noguchi, K. Fukuoka, K. Kusaba, and T. Atou, in *Shock Compression of Condensed Matter* (Ref. 2); Y. Noguchi, K. Kusaba, K. Fukuoka, and Y. Syono, Geophys. Res. Lett. **23**, 1469 (1996).

[6] R. Jeanloz and A. Rudy, J. Geophys. Res. **92**, 11 433 (1987).

[7] S. L. Webb, I. Jackson, and J. D. F. Gerald, Phys. Earth Planet. Inter. **52**, 117 (1988).

[8] R. Jeanloz, T. J. Ahrens, H. K. Mao, and P. M. Bell, Science **206**, 829 (1979).

[9] Y. Sato and R. Jeanloz, J. Geophys. Res. **86**, 11 773 (1981).

[10] L. Liu and W. A. Bassett, J. Geophys. Res. **77**, 4934 (1972).

[11] S. T. Weir, Y. K. Vohra, and A. L. Ruoff, Phys. Rev. B **33**, 4221 (1986).

[12] T. S. Duffy, R. J. Hemley, and H. K. Mao, Phys. Rev. Lett. **74**, 1371 (1995).

[13] R. Jeanloz and T. J. Ahrens, Geophys. J. R. Astron. Soc. **62**, 505 (1980).

[14] T. Yagi, K. Fukuoka, H. Takei, and Y. Syono, Geophys. Res. Lett. **15**, 816 (1988).

[15] E. Knittle and R. Jeanloz, Geophys. Res. Lett. **13**, 1541 (1986).

[16] E. Knittle, R. Jeanloz, A. C. Mitchell, and W. J. Nellis, Solid State Commun. **59**, 513 (1986).

[17] Y. W. Fei and H. K. Mao, Science **266**, 1678 (1994).

[18] H. K. Mao *et al.*, Phys. Earth Planet. Inter. **96**, 135 (1996).

[19] R. E. Cohen, I. I. Mazin, and D. G. Isaak, Science **275**, 654 (1997).

[20] R. G. Parr and W. Yang, *Density-Functional Theory of Atoms and*

Molecules (Oxford, New York, 1989).
[21] K. J. Chang and M. L. Cohen, Phys. Rev. B **30**, 4774 (1984).
[22] K. T. Park, K. Terakura, and Y. Matsui, Nature (London) **336**, 670 (1988).
[23] R. J. Hemley and R. E. Cohen, Annu. Rev. Earth Planet Sci. **20**, 553 (1992).
[24] D. G. Isaak, R. E. Cohen, M. J. Mehl, and D. J. Singh, Phys. Rev. B **47**, 7720 (1993).
[25] V. L. Moruzzi, J. F. Janak, and A. R. Williams, *Calculated Electronic Properties of Metals* (Pergamon, New York, 1978).
[26] J. P. Perdew, in *Electronic Structure of Solids*, edited by P. Ziesche and H. Eschrig (Akademie-Verlag, Berlin, 1991).
[27] D. M. Sherman and H. J. F. Jansen, Geophys. Res. Lett. **22**, 1001 (1995).
[28] D. M. Sherman, Geophys. Res. Lett. **16**, 515 (1989).
[29] Z. Fang, K. Terakura, H. Sawada, T. Miyazaki, and I. Solovyev, Phys. Rev. Lett. **81**, 1027 (1998).
[30] I. V. Solovyev, P. H. Dederichs, and V. I. Anisimov, Phys. Rev. B **50**, 16 861 (1994).
[31] R. Car and M. Parrinello, Phys. Rev. Lett. **55**, 2471 (1985).
[32] D. Vanderbilt, Phys. Rev. B **41**, 7892 (1990).
[33] D. R. Hamann, M. Schlüter, and C. Chiang, Phys. Rev. Lett. **43**, 1494 (1979).
[34] R. D. King-Smith and D. Vanderbilt, Phys. Rev. B **49**, 5828 (1994).
[35] P. Focher and G. L. Chiarotti, *Progress in Computational Physics of Matter: Methods, Software and Applications* (World Scientific, Singapore, 1995).
[36] K. Terakura, T. Oguchi, A. R. Williams, and J. Kubler, Phys. Rev. B **30**, 4734 (1984).
[37] F. D. Murnaghan, Proc. Natl. Acad. Sci. USA **30**, 244 (1944).
[38] I. V. Solovyev and K. Terakura, Phys. Rev. B (to be published).
[39] J. van Elp, R. H. Potze, H. Eskes, R. Berger, and G. A. Sawatzky, Phys. Rev. B **44**, 1530 (1991).
[40] J. Kanamori, Prog. Theor. Phys. **17**, 177 (1957); **17**, 197 (1957).
[41] P. Bruno, Phys. Rev. B **39**, 865 (1993).
[42] We use the nearly orthogonal ASA-LMTO method [O. Gunnarsson, O. Jepsen, and O. K. Andersen, Phys. Rev. B **27**, 7144 (1983)], where the atomic radii were taken as 2.785 (Fe) and 2.2 a.u. (O), and the valence states were expanded in terms of Fe($4sp$,$3d$) and O($2sp$) basis orbitals. The SOC was included in the pseudoperturbation manner.
[43] I. V. Solovyev, A. I. Liechtenstein, and K. Terakura, J. Magn. Magn. Mater. **185**, 118 (1998).
[44] O. Gunnarsson, E. Koch, and R. M. Martin, Phys. Rev. B **54**, R11 026 (1996).
[45] R. W. G. Wyckof, *Crystal Structures* (Interscience, New York, 1963), Vol. 1, p. 124.
[46] R. D. Shannon and C. T. Prewitt, Acta Crystallogr., Sect. B: Struct. Crystallogr. Cryst. Chem. **25**, 925 (1969).
[47] J. C. Slater, *Quantum Theory of Molecules and Solids* (McGraw-Hill Inc., New York, 1965), Vol. 2.